INTERNATIONAL JOURNAL FOR NUMERICAL METHODS IN FLUIDS, VOL. 5, 709–725 (1985)

ISOTHERMAL FLOW PAST A BLOWING SPHERE

K. A. CLIFFE AND D. A. LEVER

Theoretical Physics Division, AERE, Harwell, Oxfordshire, OX11 0RA

SUMMARY

Steady, axisymmetric, isothermal, incompressible flow past a sphere with uniform blowing out of the surface is investigated for Reynolds numbers in the range 1 to 100 and surface velocities up to 10 times the free stream value. A stream-function–velocity formulation of the flow equations in spherical polar co-ordinates is used and the equations are solved by a Galerkin finite-element method. Reductions in the drag coefficients arising from blowing are computed and the effects on the viscous and pressure contributions to the drag considered. Changes in the surface pressure, surface vorticity and flow patterns for two values of the Reynolds number (1 and 40) are examined in greater detail. Particular attention is paid to the perturbation to the flow field far from the sphere.

KEY WORDS Isothermal Laminar Flow Finite Elements Flow Past a Sphere Surface Blowing Drag

1. INTRODUCTION

An understanding of the motion and evaporation of fuel droplets is essential to the development of physical and numerical models describing the combustion of liquid fuel sprays in furnaces or internal combustion engines. The models used to date have either neglected the effects of motion[1] or incorporated simplified models: the model for drag is appropriate to steady isothermal flow past a sphere, and that for evaporation is for a single isolated droplet in a stagment ambient fuel-vapour atmosphere, both models are adjusted to coincide with accepted correlations.[2,3]

In this paper we discuss a numerical solution of the equations for isothermal, incompressible, laminar flow past a sphere with uniform normal blowing over the surface. These calculations incorporate qualitatively the effects of evaporation and they clearly show the important physical processes in the flow. However, the assumptions of uniform blowing and constant properties are gross simplifications of the actual flow, and so further work will comprise full heat and mass transfer calculations. As estimates of numerical accuracy are easier to find for the isothermal calculations described here, the present results will provide invaluable experience and will be used to validate subsequent solutions of the thermal problem.

Isothermal flow past the sphere is described by two parameters: the Reynolds number Re and the blowing number Λ. The Reynolds number is defined as

$$Re = d\,U\rho/\mu, \tag{1}$$

where d is the droplet diameter, U its velocity relative to the surrounding gas, ρ the density and μ the dynamic viscosity of the gas. Typical values of Re are less than 1000; for example a $100\,\mu$m drop moving at $8\,\mathrm{ms}^{-1}$ through kerosene vapour at 1000 K gives $Re = 160$. Steady isothermal flow around a sphere is stable at low Reynolds number; it becomes unstable at a Reynolds number of 130, when oscillations appear in the wake.[4] Therefore for $Re \lesssim 130$ the drag can

0271–2091/85/080709–17$01.70

Received September 1984
Revised March 1985

be determined by examining steady flow past a spherical drop. The blowing number is a measure of the strength of the evaporation and is defined as

$$\Lambda = V/U, \tag{2}$$

where V is the radial gas velocity at the droplet surface. For an evaporating drop, this is determined by the temperature gradient and the thermal conductivity in the vapour at the droplet surface, and by the latent heat of vaporization. As an example, for small Reynolds numbers Λ is approximately $2/Re$ for a kerosene droplet at 480 K moving through vapour at 1000 K. This shows that the blowing velocity can be comparable to the droplet velocity.

There have been a number of calculations of the drag on cylinders and spheres in steady, isothermal flow. The most extensive calculations for non-blowing cylinders are those of Fornberg.[5] Solutions for non-blowing spheres include those of Hamielec *et al.*[6] Le Clair *et al.*,[7] Dennis and Walker,[8] Renksizbulut,[9] Renksizbulut and Yuen[10] and Cliffe and Lever.[11,12] In the last two papers a method similar to the one described here is used, a variety of grids are considered, and error estimates presented. Fewer authors have considered blowing spheres. The calculations by Hamielec *et al.*[6] and Chuchottaworn *et al.*[13] are inaccurate because the position of the outer boundary of the solution region is rather too close to the sphere. Renksizbulut and Yuen[9,10] have considered both isothermal flow past a non-blowing sphere and the full heat and mass transfer within flow around an evaporating drop. However, they only report[9] on the use of a single finite-difference mesh and they comment that their results are only accurate to within a few per cent.

Finally Dukowicz[14] has found an analytic solution for the case of low Reynolds number ($Re \lesssim 1$) but arbitrary blowing Reynolds number ($R_B = Re\Lambda$). This provides a useful comparison with our numerical results.

In the next section we discuss the mathematical formulation of the equations, boundary conditions and the drag calculation; and then in Section 3 the finite-element numerical method used for the solution is briefly described. Finally in Section 4 we present the results of the calculations by showing how surface blowing affects the drag coefficient, the flow streamlines, vorticity contours and values of the surface vorticity and surface pressure. The Reynolds numbers used are in the range 1 to 100; for $Re = 1$, Λ varies from 0 to 10, whereas for $Re = 100$, Λ ranges from 0 to 1.

2. MATHEMATICAL MODEL

In this section we describe the mathematical formulation used to model flow around a blowing sphere, attending to the form of the Navier–Stokes equations, the co-ordinate system and the boundary conditions. In particular we discuss the boundary condition to be applied at a large distance from the sphere. Formulae for calculating the drag coefficient, surface pressure and jump in stream function across the wake are also presented.

2.1. The equations and boundary conditions

The Navier–Stokes equations can be formulated in terms either of the stream function and the vorticity or of the velocity and pressure. For the case of isothermal external flows there are advantages in using the stream-function–vorticity form that result from the nature of the flow in the region outside the wake and far from the body. Here viscous forces are negligible and the flow is essentially irrotational, so the vorticity is very small and the stream-function–vorticity equations simplify to a single linear, elliptic equation for the stream function. With the velocity–

pressure form, the equations are still non-linear in the inviscid region, being essentially the Euler equations. In addition, it is somewhat easier to develop and apply a physically meaningful boundary condition for the stream function than for the velocities. The details of this boundary condition are discussed below.

It is natural to use spherical polar co-ordinates (r, θ, ϕ), and with axisymmetry, the equations for the stream function and vorticity are

$$\frac{1}{\sin\theta}\frac{\partial^2\psi}{\partial r^2}+\frac{1}{r^2}\frac{\partial}{\partial\theta}\frac{1}{\sin\theta}\frac{\partial\psi}{\partial\theta}=-r\zeta, \tag{3}$$

$$\frac{1}{r^2\sin\theta}\frac{\partial\psi}{\partial\theta}\frac{\partial\zeta}{\partial r}-\frac{1}{r^2\sin\theta}\frac{\partial\psi}{\partial r}\frac{\partial\zeta}{\partial\theta}-\frac{\zeta}{r^3\sin\theta}\frac{\partial\psi}{\partial\theta}+\frac{\zeta\cot\theta}{r^2\sin\theta}\frac{\partial\psi}{\partial r}$$
$$-\frac{2}{Re}\left\{\frac{1}{r^2}\frac{\partial}{\partial r}r^2\frac{\partial}{\partial r}\zeta+\frac{1}{r^2\sin\theta}\frac{\partial}{\partial\theta}\sin\theta\frac{\partial\zeta}{\partial\theta}-\frac{\zeta}{r^2\sin^2\theta}\right\}=0, \tag{4}$$

where ψ is the stream function, ζ the vorticity and Re the Reynolds number (1). The equations have been made dimensionless by dividing distances by the radius of the sphere and velocities by the free stream velocity. These equations are solved in the region given by $1\leqslant r\leqslant r_\infty$ and $0\leqslant\theta\leqslant\pi$. For computational purposes we introduce the variable $\xi=\ln(r)$ and treat ξ and θ as the independent variables. This change of variables produces a natural compression, in real space, of the grid lines near the sphere.

Equations (3) and (4) must be supplemented by appropriate boundary conditions. Along the upstream symmetry axis ($\theta=\pi$), ψ and ζ are both zero. Around the surface of the sphere ($r=1$), the zero tangential velocity condition implies $\partial\psi/\partial r$ is zero, and the uniform blowing velocity implies that ψ decreases round sphere and is given by

$$\psi=-\Lambda(1+\cos\theta)\quad\text{at}\quad r=1. \tag{5}$$

Along the downstream symmetry axis ($\theta=0$), ζ is again zero and ψ constant (-2Λ).

One of the difficulties associated with external flow calculations is the specification of boundary conditions far from the body (sphere in this case). This question is much more acute in two-dimensional calculations where the disturbance to the free stream flow decays more slowly than in three dimensions. Nevertheless, insufficient care can lead to inaccurate results even in three-dimensional calculations.

The boundary condition on vorticity far from the sphere is that $\zeta=0$ for $\pi/2\leqslant\theta\leqslant\pi$ and $\partial\zeta/\partial r=0$ for $0\leqslant\theta\leqslant\pi/2$. Vorticity is created at the surface of the sphere and then diffuses away from the surface and is convected downstream by the flow. The part of the boundary $\pi/2\leqslant\theta\leqslant\pi$ at $r=r_\infty$ is the inflow boundary and the above boundary condition expresses the fact that there is no vorticity in the free stream. The boundary condition applied on $0\leqslant\theta\leqslant\pi/2$ is numerically convenient, and because of the form of the vorticity equation, any error introduced by this condition decays exponentially away from the boundary.

Most previous calculations of flow past a non-blowing sphere have employed a free stream boundary condition on the stream function at $r=r_\infty$. This implies that r_∞ is sufficiently large so that at $r=r_\infty$ the stream function is unaffected by the presence of the sphere. The error introduced by this boundary condition decreases as r_∞ increases, but for practical values of r_∞ it may still be significant. For the blowing sphere we write

$$\psi=\tfrac{1}{2}r^2\sin^2\theta-\Lambda(1+\cos\theta)+\psi_p, \tag{6}$$

where $\frac{1}{2}r^2\sin^2\theta$ is the stream function for the uniform flow in the absence of the sphere and

mass source, $-\Lambda(1+\cos\theta)$ is the stream function for a point source emitting at the same rate as the blowing sphere, and ψ_p is the perturbation due to the presence of the sphere. Then the boundary condition that the stream function far from the sphere is not affected by the presence of the sphere, implies that

$$\psi_p = 0 \quad \text{at} \quad r = r_\infty. \tag{7}$$

A better boundary condition may be developed by noting that at large distances from the sphere and for arbitrary Reynolds number, the perturbed component of the flow has two parts.[4] There is an inflow in the wake region which is associated with the momentum defect: the momentum removed from the free stream which produces the drag on the sphere. To compensate for this inflow there is a uniform radial outward flow which, at large distances, looks like the flow from a point source of mass at the sphere. At sufficiently large distances the perturbed flow is radial; this implies that

$$\frac{\partial \psi_p}{\partial r} = 0. \tag{8}$$

The condition (8) is much easier to apply in a stream-function–vorticity formulation than in a velocity–pressure formulation. This condition has been used previously by Fornberg[5] in a study of flow past a circular cylinder. It has a more secure physical basis than the boundary condition (7) and we thus expect to be able to apply it closer to the sphere.

2.2. *The drag coefficient and surface pressure*

In addition to the dependent variables of (3) and (4)—the stream function and vorticity—certain other quantities reveal important characteristics of the flow. The drag coefficient is of particular importance; it is related to the drag on the sphere by

$$C_D = \frac{D}{\frac{1}{2}\rho U^2 A}, \tag{9}$$

where D is the force in the direction of the flow, and A is the cross-sectional area normal to the flow ($\pi d^2/4$). The force on the sphere can be split into three parts: the viscous, pressure and thrust components,

$$\begin{aligned} \mathbf{D} &= \mathbf{D}_v + \mathbf{D}_p + \mathbf{D}_T \\ &= \int_{\text{sphere}} 2\mu \mathbf{e}\cdot d\mathbf{S} - \int_{\text{sphere}} p\, d\mathbf{S} - \int_{\text{sphere}} \rho \mathbf{u}(\mathbf{u}\cdot d\mathbf{S}), \end{aligned} \tag{10}$$

where $\mathbf{e}$ is the rate-of-strain tensor, p the fluid pressure and $\mathbf{u}$ the fluid velocity (with radial and tangential components u_r and u_θ). The viscous component of the drag coefficient (9) can be expressed in terms of the dimensionless variables of (3) and (4) as

$$C_v = -\frac{8}{Re}\int_0^\pi (\zeta \sin^2\theta)_{r=1}\, d\theta. \tag{11}$$

From the θ component of the momentum equation, it can be shown that at the surface of the sphere, where $u_\theta = 0$,

$$\left(\frac{\partial p}{\partial \theta}\right)_{r=1} = \frac{2}{Re}\left(\zeta + \frac{\partial \zeta}{\partial r}\right) - u_r\left(\zeta + \frac{\partial u_r}{\partial \theta}\right). \tag{12}$$

Using (12), the pressure or form component of the drag coefficient can be written

$$C_p = \frac{4}{Re}\int_0^{\pi}\left(\zeta + \frac{\partial\zeta}{\partial r} - \frac{Reu_r}{2}\zeta\right)_{r=1}\sin^2\theta\,\mathrm{d}\theta - \frac{C_T}{2}. \tag{13}$$

However in the case considered here, the blowing is uniform around the sphere, so the thrust component, C_T, is zero and (13) can be rewritten as

$$C_p = \frac{4}{Re}\int_0^{\pi}\left(\zeta + \frac{\partial\zeta}{\partial r} - \frac{Re\Lambda}{2}\zeta\right)_{r=1}\sin^2\theta\,\mathrm{d}\theta. \tag{14}$$

Another quantity of interest is the surface pressure. First, integration of the radial component of the momentum equation along the upstream dividing streamline ($\theta = \pi$) gives the value at the front of the sphere to be

$$p_\pi = p_\infty + \tfrac{1}{2}(1-\Lambda^2) + \frac{4}{Re}\int_0^{\infty}\left(\frac{\partial\zeta}{\partial\theta}\right)_{\theta=\pi}\mathrm{d}\xi, \tag{15}$$

where $\xi = \ln r$ and p_∞ is the pressure far from the sphere. Then integration of (12) around the sphere, recalling $\partial u_r/\partial\theta = 0$, gives

$$p(\theta) = p_\pi + \int_\pi^{\theta}\left(\left(\frac{2}{Re} - \Lambda\right)\zeta + \frac{2}{Re}\frac{\partial\zeta}{\partial r}\right)_{r=1}\mathrm{d}\theta. \tag{16}$$

If Λ is set to zero in the above expressions ((11), (14)–(16)), they correspond to those of Dennis and Walker,[8] whose definition of C_D is, however, half the one used here (9).

2.3. *The momentum defect in the wake*

Finally, we investigate how blowing modifies the relationship between the drag and the momentum defect associated with the inflow in the wake. For this, the integral form of the momentum equation is applied in precisely the same manner as described by Batchelor[4] for the non-blowing case. With uniform blowing there is no net flux of momentum out of the sphere, and so the only alteration to the argument is the inclusion of the flux out of the sphere in the mass conservation equation. This gives

$$D = -\pi\rho U^2\Lambda d^2 + \rho UQ, \tag{17}$$

where Q is the volume defect. Moreover, Q can be related to the jump in the perturbation stream function, ψ_p (6), across the wake

$$Q = -\tfrac{1}{2}\pi d^2 U[\psi_p]_{\theta=0}. \tag{18}$$

So substitution of (9) and (18) into (17) gives

$$[\psi_p]_{\theta=0} = -2\Lambda - \tfrac{1}{4}C_D, \tag{19}$$

indicating that the jump in ψ_p is rather larger in the blowing case. The corresponding form of ψ_p far from the sphere is

$$\psi_p = \begin{cases} 0, & \theta = 0 \\ -(\Lambda + \tfrac{1}{8}C_D)(1+\cos\theta), & \theta > 0 \end{cases}, \quad r \to \infty. \tag{20}$$

Equation (17) gives the strength of the apparent source of mass at the sphere arising from the volume defect in the wake to be $Q = \pi d^2 V + D/\rho U$. This is in addition to the actual source $\pi d^2 V$

arising from the uniform blowing, and so, outside the wake, the total apparent source is

$$2\pi d^2 V + D/\rho U, \tag{21}$$

that is the sum of the contribution from the drag found in the non-blowing case and twice the flux arising from the uniform blowing at the surface.

3. NUMERICAL METHOD

A Galerkin finite-element method using nine-node biquadratic elements is used to discretize equations (3) and (4) with ξ and θ as independent variables. The method is similar to that of Tong[15] and has been used previously by Winters and Cliffe[16] and Cliffe and Lever,[11,12] among others.

The only difficulty, which therefore requires specific attention, is the imposition (8) of the zero normal derivative far from the sphere as an appropriate boundary condition on the perturbation steam function. The obvious solution is to use the perturbation stream function ψ_p as the second dependent variable (the first being vorticity), since zero normal derivative is then a 'natural' boundary condition. ψ_p satisfies equations derived from (3) and (4) by substitution of analytic expressions for the undisturbed stream and point source stream functions (equation (6)). In particular, the stream function for the undisturbed stream is given by

$$\psi_{us} = \tfrac{1}{2} r^2 \sin^2 \theta. \tag{22}$$

Unfortunately, the usual finite-element treatment of ψ_{us} appears to be unsatisfactory. We found that the solution for the surface vorticity exhibited 'wiggles' particularly in the regions near $\theta = 0$ and $\theta = \pi$. We attributed these 'wiggles' to the fact that the finite-element interpolation of $\sin^2 \theta$ is not very smooth, and the $1/\sin\theta$ terms in equations (3) and (4) amplify the effect. Since the surface values of stream function are fixed, this shows up in the surface vorticity.

The expedient we adopted is to replace the analytical solution for ψ_{us} which is the cause of the problem, by a finite-element approximation, which is obtained by solving equation (3) with $\zeta = 0$ and appropriate Dirichlet boundary conditions at the surface of the sphere and at the boundary at 'infinity'. We then have

$$\hat{\psi} = \hat{\psi}_{us} - \Lambda(1 + \cos\theta) + \hat{\psi}_p \tag{23}$$

where $\hat{}$ denotes finite-element approximation. Equation (3) is then regarded as an equation for $\hat{\psi}_p$, and the above treatment removes the wiggles in surface vorticity.

As a result of solving equations dependent upon $\hat{\psi}_{us}$ for $\hat{\psi}_p$ and $\hat{\zeta}$, care is needed to ensure that the condition that $\hat{\psi}_p$ has zero normal derivative on the boundary far from the sphere is applied correctly. In particular, the approximation to the normal derivative of $\hat{\psi}_{us}$ on the boundary must ensure that the terms in the finite-element equation involving $\hat{\psi}_{us}$ cancel. This is known as the 'consistent' finite-element approximation to the derivative. If the consistent form of the derivative is not used, the problems encountered near the sphere move to the boundary at 'infinity', and large errors result in the stream function there.

The non-linear algebraic equations for the nodal values of stream function and vorticity are solved by Newton's method. The linear system at each iteration is solved using the frontal method.[17]

We believe that the drag calculations described in the next section all have an error of less than 1 per cent and many are more accurate. A variety of uniform grids were used in the calculations, specified by three quantities: n_θ the number of elements in the θ direction, n_ξ the number of elements radially and ξ_∞ the position of the outer boundary where the condition (8)

was applied. Different values of these quantities are needed to obtain the above accuracy for different ranges of Re and Λ.

In the absence of blowing, it is quite easy to obtain values of the viscous component C_v (11) that vary little with grids used. Values of C_p (14) that are independent of ξ_∞ or n_θ can also be obtained; however independence of n_ξ is not as easy to achieve. Since the expression for C_v only contains values of ζ on the surface of the sphere, we expect $O(h^3)$ convergence, where h is the element size in the radial direction (ξ_∞/n_ξ). However, as C_p involves radial derivatives of ζ, we expect an $O(h^2)$ component in the error. As a result C_p converges more slowly. So the results of different grids are used to calculate an extrapolated value of the drag coefficient, using an expression of the form

$$v(h) = e + \alpha h^2 + \beta h^3. \tag{24}$$

Three grids are used to give e, α and β; typical values of n_ξ are 60, 80 and 100. This is not a strictly rigorous refinement procedure; successive bisection in both directions for all values of ξ_∞ is not practical.

When there is significant blowing and the blowing Reynolds number ($R_B = Re\Lambda$) is large, the major contribution to C_p comes from the final term in (14), and

$$C_p \sim \frac{R_B}{4} C_v \gg C_v. \tag{25}$$

As a result the extrapolation procedure is no longer necessary and 50–80 radial elements are sufficient. However, the vorticity is now blown away from the sphere, so care has to be taken that the outer boundary of the solution region (ξ_∞) is far enough away. Whereas for most non-blowing cases $\xi_\infty = 3{\cdot}6$ ($r_\infty = 36{\cdot}6$) suffices, with significant blowing $\xi_\infty = 4{\cdot}2$ ($r_\infty = 66{\cdot}7$) is required.

This leads to one final problem: the resolution of the narrow wake at large Re. In real space, the wake grows as[4]

$$s^2 \sim \frac{x}{Re}, \tag{26}$$

where s is the distance from the axis, and x the distance along the axis. When expressed in terms of $\theta(= \tan^{-1} s/x)$ and $\xi(= \ln r)$, this becomes

$$\theta \sim (Re\, e^{\xi})^{-1/2}. \tag{27}$$

So with large ξ_∞ and Re, more elements in the θ direction are required to adequately resolve the wake. For the cases described in the next section with $Re = 100$ and $\Lambda \gtrsim 0{\cdot}3$, 40 elements are used, rather than 20 or 30 as in the majority of other cases.

4. DISCUSSION OF RESULTS

4.1. The drag coefficient

The drag coefficient C_D and its two components C_v (11) and C_p (14) have been calculated from finite-element flow solutions for a range of Re and Λ. Values of Re were in the range 1 to 100; for $Re = 1$, Λ was varied from 0 to 10, but as Re was increased the maximum value of Λ considered decreased, until for $Re = 100$, Λ ranged from 0 to 1. The results are shown in Figure 1 where C_D, C_p and C_v are plotted as functions of Λ for $Re = 1$, 2, 5, 10, 40 and 100, and are summarized in Table I. For the parameter ranges considered, the effect of increasing Λ is always to decrease the drag.

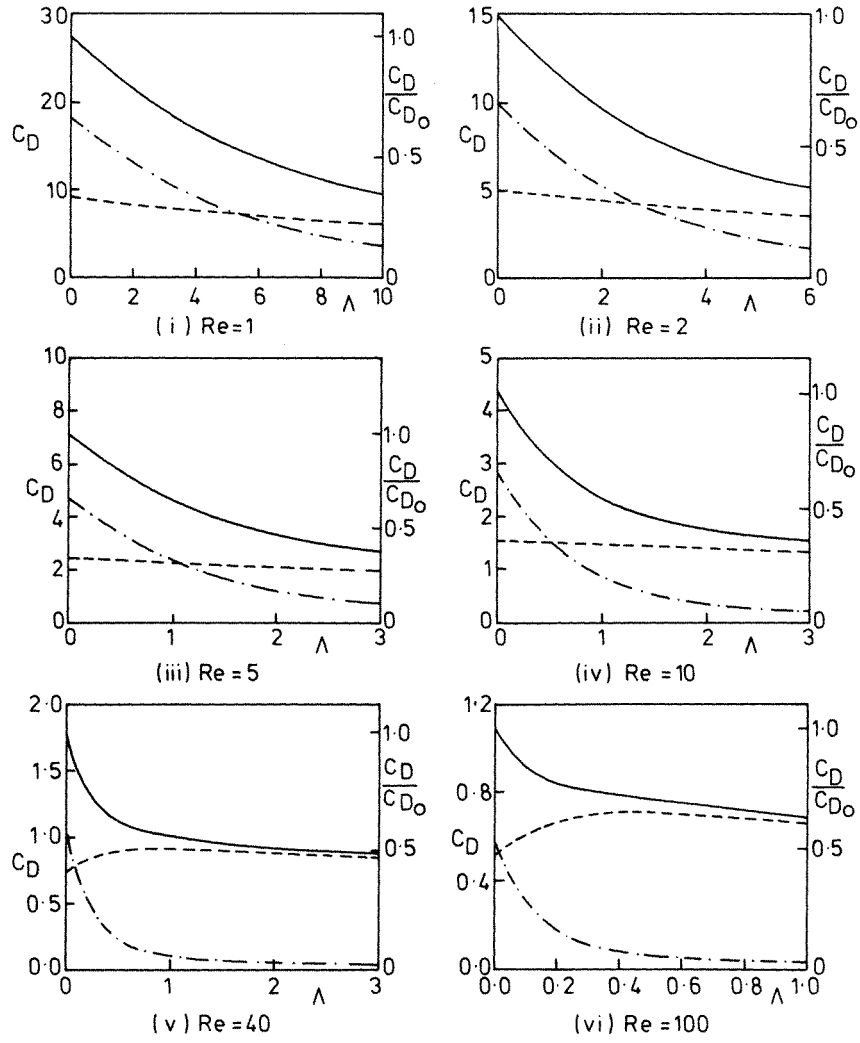

Figure 1. The drag coefficient C_D as a function of blowing number Λ for $Re = 1, 2, 5, 10, 40$ and 100.———C_D, - - - C_p, —·—·C_v. The right hand ordinate is C_D/C_{D_0}, where C_{D_0} is the coefficient at the same Reynolds number and $\Lambda = 0$

Table I. The drag coefficient for a range of Reynolds numbers (Re) and blowing numbers (Λ).

	Λ			
Re	0	0·3	1·0	3·0
1	27·32	26·31	24·09	18·87
2	14·92	13·93	11·09	7·90
5	7·14	6·21	4·60	2·66
10	4.31	3.46	2.322	1·540
40	1·789	1·244	1·044	0·860
100	1·088	0·805	0·685	—

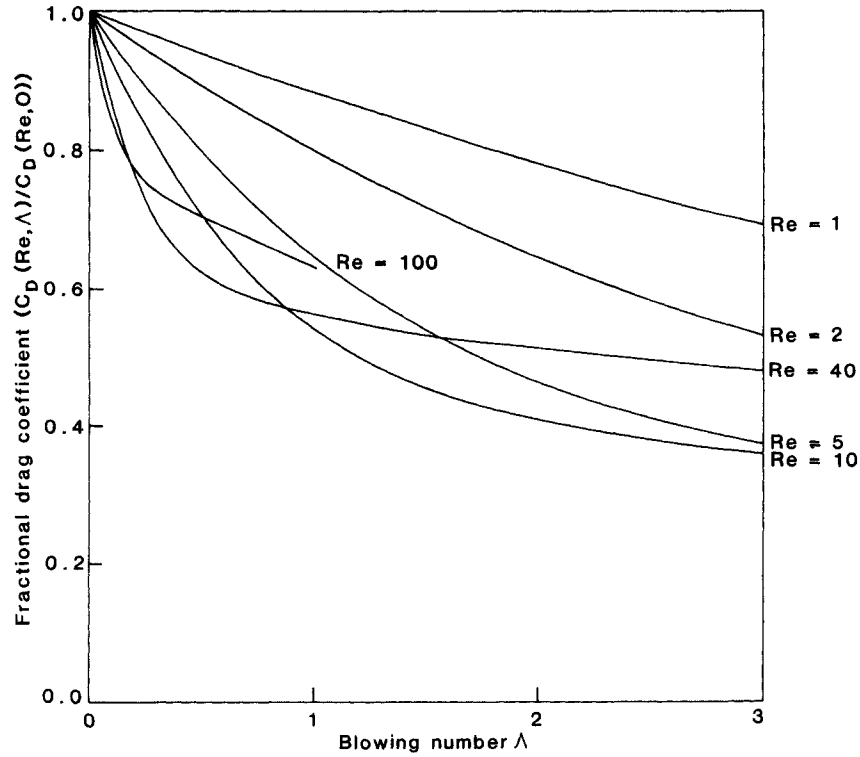

Figure 2. The drag coefficient divided by its value at the same Reynolds number in the absence of blowing, as a function of blowing number; for various Reynolds numbers

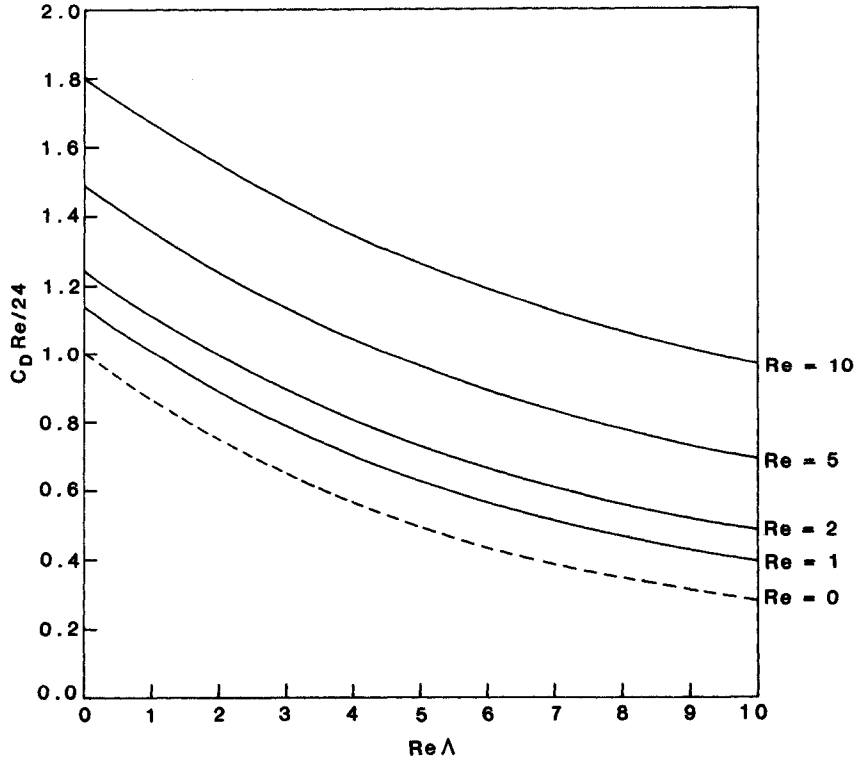

Figure 3. The drag coefficient (C_D) divided by the Stokes drag ($24/Re$), as a function of blowing Reynolds number ($Re\Lambda$); for various Reynolds numbers. - - - low Reynolds number analytic solution of Dukowicz[14]

In the absence of blowing and at low Re, $C_v = 2C_p$. As Re increases, the difference between C_p and C_v decreases until at $Re = 100$ they are almost equal. Increasing Λ results in a rapid fall of C_v, as the vorticity is blown away from the surface and is drastically reduced. When $Re\Lambda$ is large, (25) is satisfied and $C_v \sim 4C_p/Re\Lambda \ll C_p$. Indeed an examination of the numerical results suggests that $C_v \sim 4C_D/Re\Lambda$ is an even more accurate approximation. At the lower values of Re, C_p also falls steadily with increasing Λ, although less rapidly than C_v. However for $Re = 40$ and 100, C_p initially rises, reaches a maximum and then decreases. The increase in C_p is much smaller than the fall in C_v and so C_D still decreases. This observation contradicts the argument sometimes found in the literature that the fall in C_v is compensated by a comparable rise in C_p, so that there is essentially no change in C_D. For no range of Λ is C_D approximately constant.

It might be thought that at high Re blowing would enhance boundary layer separation, increasing the drag. However, if this argument is valid, it applies outside the range of Re considered here, when the steady solutions will no longer be stable.

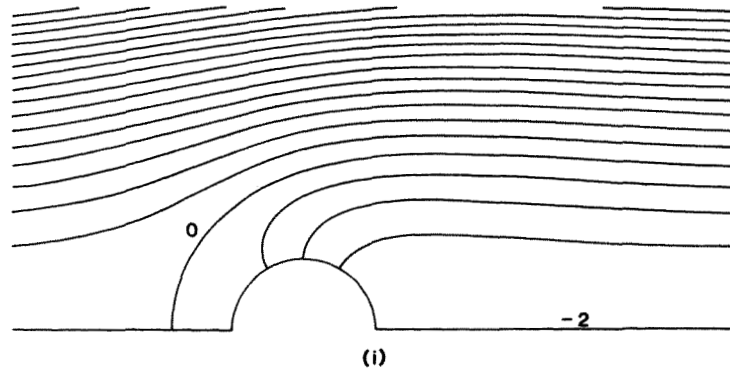

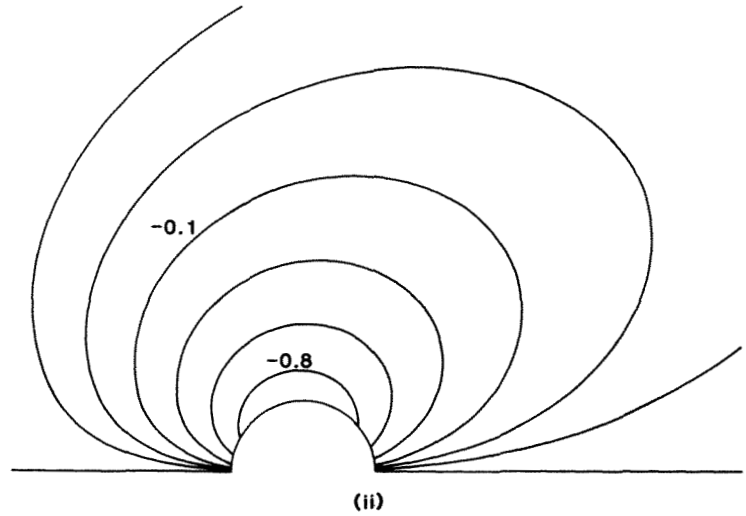

Figure 4. Flow past a sphere for $Re = 1$, $\Lambda = 1$: (i) streamlines, $\psi = 8, 7{\cdot}5, 7, \ldots, -1{\cdot}5, -2$ (in intervals of 0·5); (ii) vorticity contours, $\zeta = -0{\cdot}8, -0{\cdot}4, -0{\cdot}2, -0{\cdot}1, -0{\cdot}05, -0{\cdot}025$

In Figure 2 the drag coefficient expressed as a fraction of the value at the same Reynolds number, but in the absence of blowing (that is as a fraction of $C_{D_0} = C_D(Re, 0)$), is plotted against Λ for $Re = 1, 2, 5, 10, 40$ and 100. The Figure shows that the slope of these plots at $\Lambda = 0$ becomes steadily steeper (that is more negative) with increasing Re, but we also see that the slopes for higher Re become less steep at much lower values of Λ, and as a result the curves cross. Thus for values of Λ greater than about 0·9, the value of C_D/C_{D_0} is greater at $Re = 40$ than at $Re = 10$, and beyond $\Lambda = 1{\cdot}5$ it is greater at $Re = 40$ than at $Re = 5$.

Dukowicz[14] has found an analytic solution for small $Re (Re \lesssim 1)$ and arbitrary blowing Reynolds number ($R_B = Re\,\Lambda$). To examine the approach to his solution, the drag coefficient divided by the Stokes drag coefficient for the case of no blowing ($24/Re$) is plotted against R_B for $Re = 1$, 2, 5 and 10 in Figure 3. The curves are seen approaching his limit as Re decreases.

4.2. *Flow patterns*

To examine the effects of blowing on the flows, we focus on two values of the Reynolds number, $Re = 1$ and 40, to illustrate the difference between results at low and high values. In

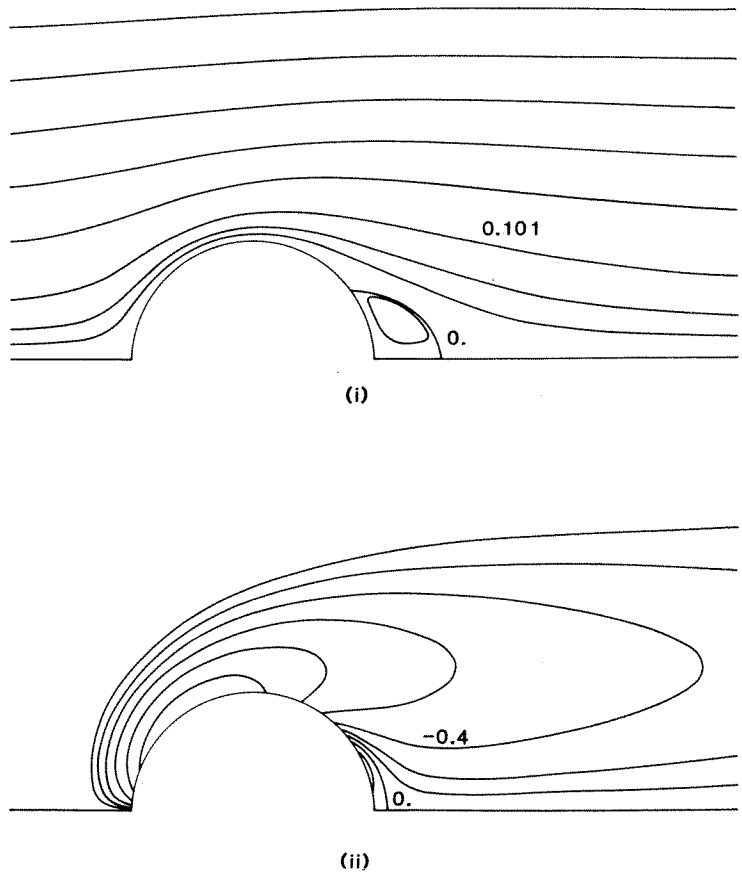

Figure 5. Flow past a sphere for $Re = 40$, $\Lambda = 0$: (i) streamlines, $\psi = 3{\cdot}65, 2{\cdot}53, 1{\cdot}62, 0{\cdot}91, 0{\cdot}41, 0{\cdot}101, 0{\cdot}025, 0{\cdot}0063, 0, -0{\cdot}0001$; (ii) vorticity contours, $\zeta = -3{\cdot}2, -1{\cdot}6, -0{\cdot}8, -0{\cdot}4, -0{\cdot}2, -0{\cdot}1, 0, 0{\cdot}1$

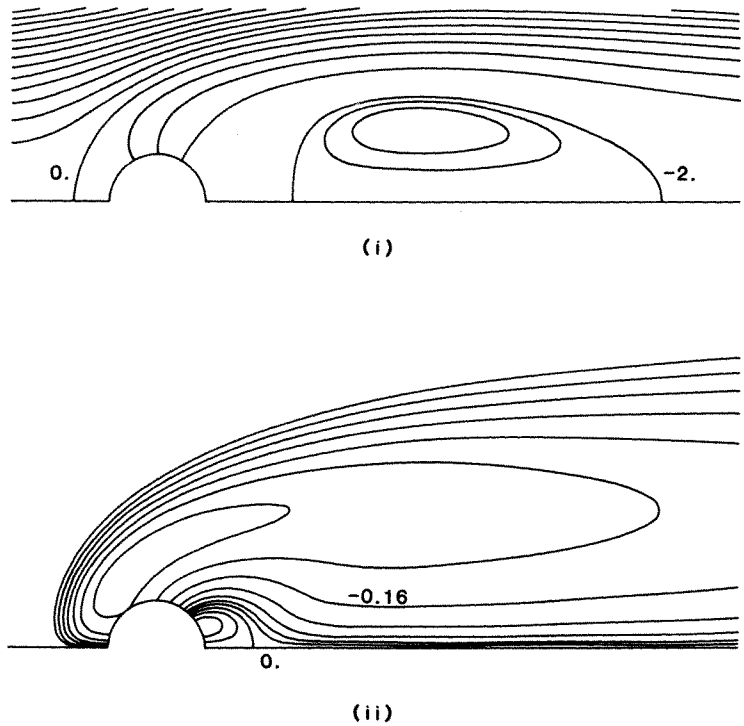

Figure 6. Flow past a sphere for $Re = 40$, $\Lambda = 1$: (i) streamlines, $\psi = 6{\cdot}5, 6, 5{\cdot}5, 5, 4{\cdot}5, 4, 3{\cdot}5, 3, 2{\cdot}5, 2, 1{\cdot}5, 1, 0{\cdot}5, 0, -0{\cdot}5, -1{\cdot}0, -1.5, -2, -2.04, -2.08$; (ii) vorticity contours, $\zeta = -0{\cdot}64, -0{\cdot}32, -0{\cdot}16, -0{\cdot}08, -0{\cdot}04, -0{\cdot}02, -0{\cdot}01, 0, 0{\cdot}01, 0{\cdot}02$

Figures 4–6 streamlines and vorticity contours close to the sphere are shown for three cases: $Re = 1$, $\Lambda = 1$; $Re = 40$, $\Lambda = 0$; $Re = 40$, $\Lambda = 1$. For $Re = 1$, $\Lambda = 1$ the vorticity contours are nearly symmetric about $\theta = \pi/2$, and are very similar to the solution without blowing. There are more significant differences between results for the two calculations with $Re = 40$. The small recirculation zone behind the sphere for $\Lambda = 0$ is replaced, at $\Lambda = 1$, by a large detached recirculation extending nearly 11 radii downstream. In addition, the magnitude of the vorticity is reduced and the vorticity is blown away from the sphere. Indeed the maximum is no longer on the surface of the sphere.

The solution for $Re = 40$, $\Lambda = 1$ is shown again in Figure 7 where two of the dependent variables ψ_p and ζ are plotted as functions of the independent variables of the computations θ and ξ ($\xi = 0$ corresponds to the surface of the sphere and $\xi = 4.2$ the outer boundary of the solution region). The narrow downstream wake at $\theta = 0$ is seen in both plots, and the large region outside the wake and far from the body where the flow is irrotational and the vorticity is zero is clear. If the free stream boundary condition (7) had been applied instead of the zero normal derivative condition (8) all the ψ_p streamlines would have been closed inside the outer boundary ($\xi = 4{\cdot}2$).

The perturbed stream function far from the sphere is shown again in Figure 8, where it is plotted in real space for $Re = 1$, $\Lambda = 1$ and $Re = 40$, $\Lambda = 1$. In Figure 9 the limiting form of ψ_p far from the sphere (20), evaluated using the computed drag coefficient, is compared with the calculated values on the outer boundary for two values of ξ_∞ (4·2 and 4·8) and for the above values of Re and Λ. Far from the sphere the wake subtends an infinitesimal value of θ, given

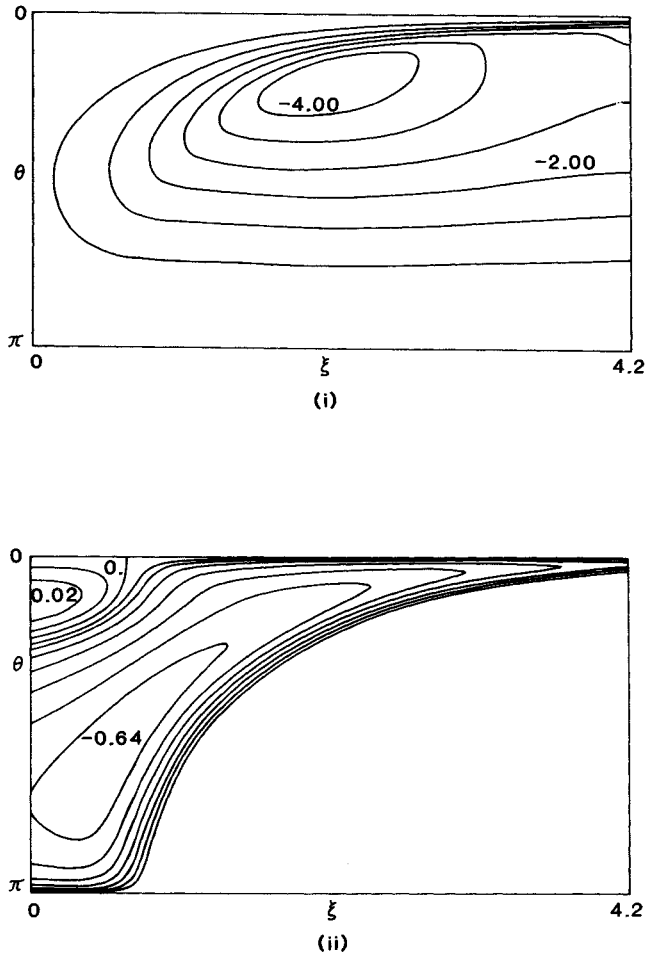

Figure 7. The perturbation stream function and vorticity contours for $Re = 40$ and $\Lambda = 1$ as functions of the independent variables for the solution: ξ and θ: (i) the perturbation stream function $\psi_p = -4{\cdot}66$, $-4{\cdot}00$, $-3{\cdot}33$, $-2{\cdot}67$, $-2{\cdot}00$, $-1{\cdot}33$, $-0{\cdot}67$; (ii) vorticity contours, $\zeta = -0{\cdot}64$, $-0{\cdot}32$, $-0{\cdot}16$, $-0{\cdot}08$, $-0{\cdot}04$, $-0{\cdot}02$, $-0{\cdot}01$, 0, 0·01, 0·02

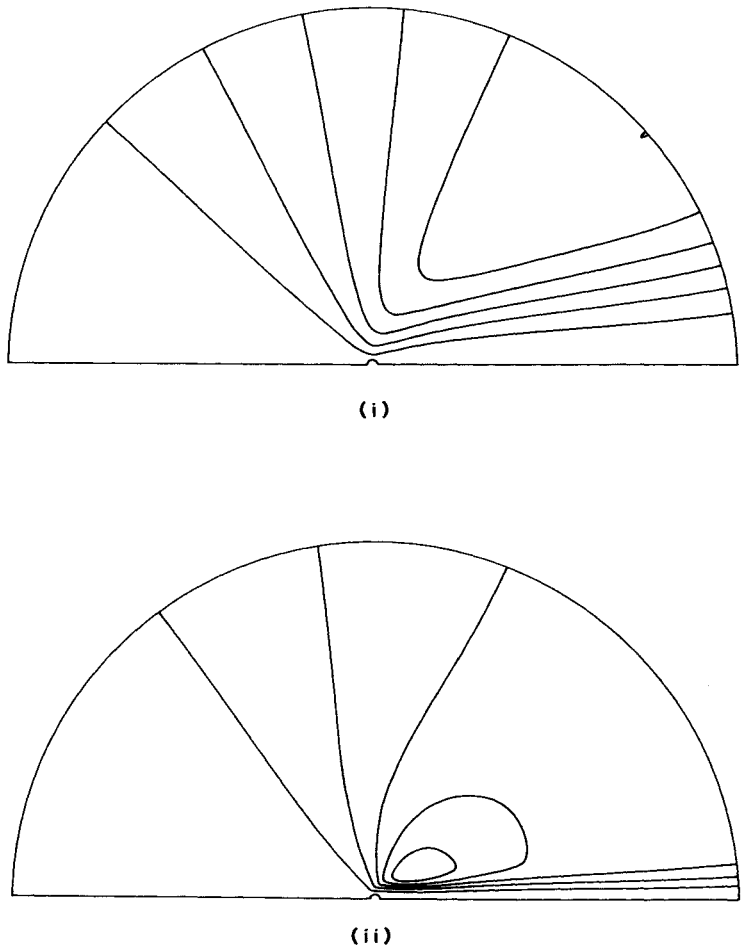

Figure 8. The perturbation stream function ψ_p in real space. The outer boundary corresponds to the edge of the computation region, $r_\infty = 66{\cdot}7$. The streamlines are equally spaced; (i) $Re = 1$, $\Lambda = 1$; (ii) $Re = 40$, $\Lambda = 1$

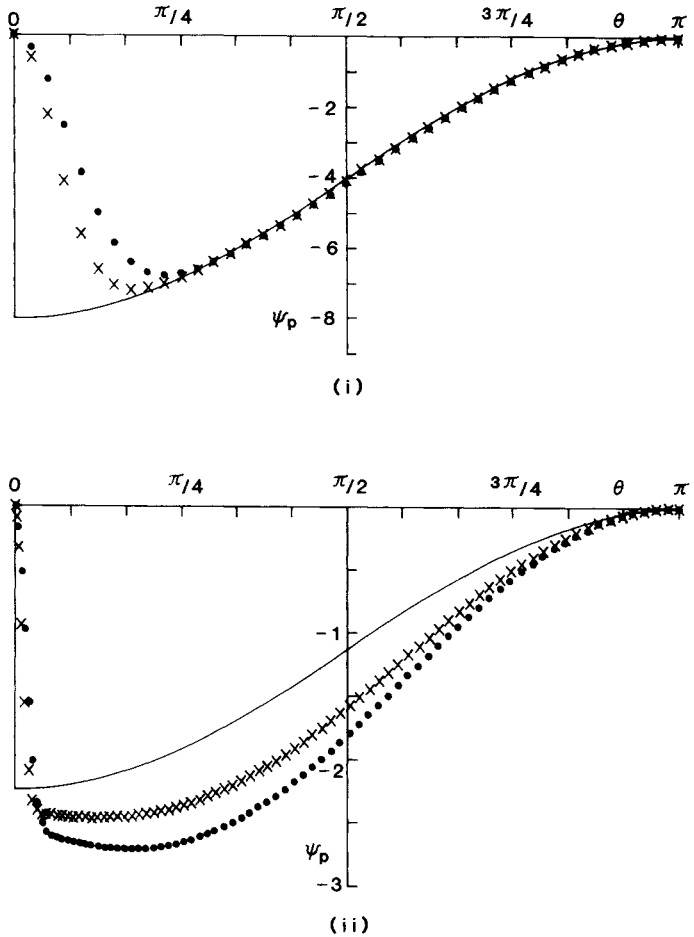

Figure 9. The perturbation stream function ψ_p along the outer boundary of the computation region as a function of $\theta(\theta = 0$ corresponds to the downstream wake). The results of numerical calculations ($\bullet$: $\xi_\infty = 4.2$, $\times$: $\xi_\infty = 4.8$) are compared with the limiting form (19) far from the sphere (solid line) for (i) $Re = 1$, $\Lambda = 1$ and (ii) $Re = 40$, $\Lambda = 1$

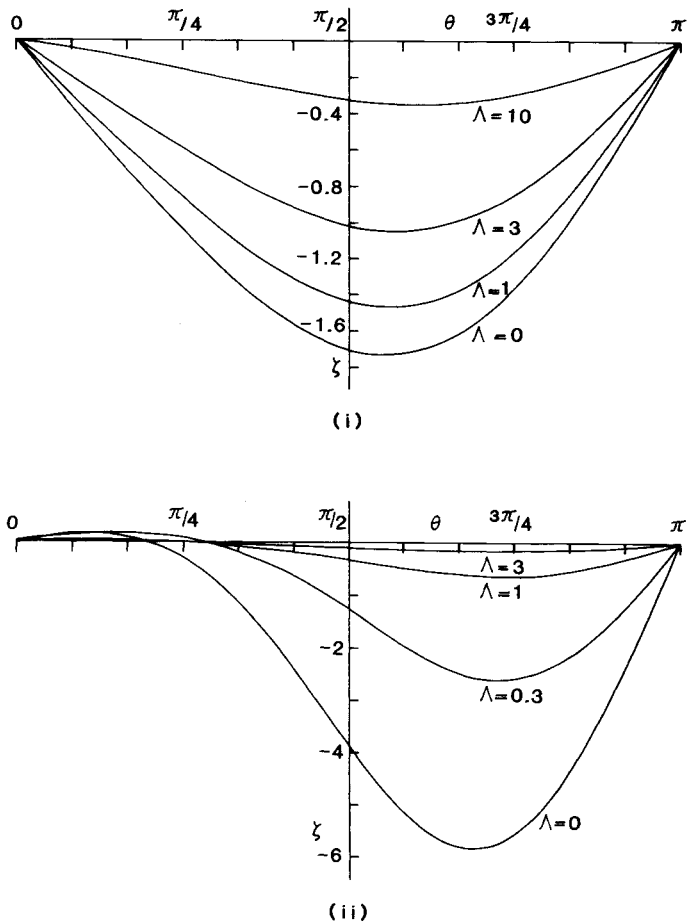

Figure 10. The vorticity ζ on the surface of the sphere as a function of $\theta(\theta = 0$ is the downstream symmetry axis) for (i) $Re = 1$ and (ii) $Re = 40$, for various blowing numbers

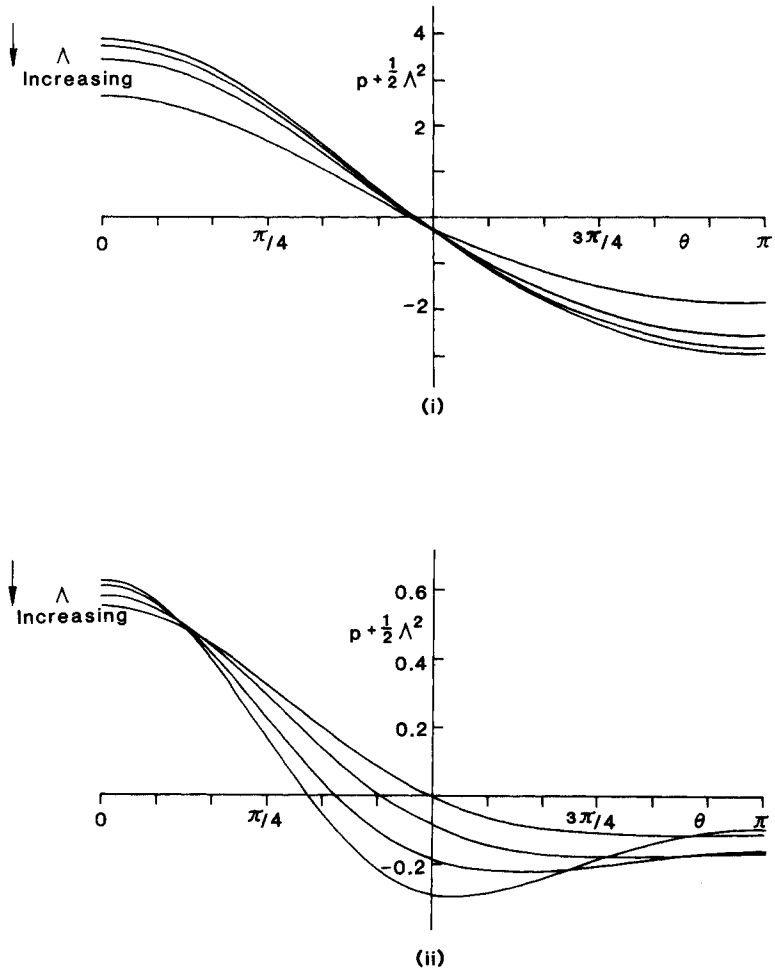

Figure 11. $p+\frac{1}{2}\Lambda^2$ on the surface of the sphere as a function of θ ($\theta = 0$ is the downstream symmetry axis) for (i) $Re = 1$, $\Lambda = 0, 1, 3, 10$ and (ii) $Re = 40$, $\Lambda = 0, 0{\cdot}3, 1, 3$

Table II. The variation of the pressure at the surface of the sphere on the upstream axis (p_π) and downstream axis (p_0) with Λ for two values of Re.

Λ	p_π	p_0	$p_\pi+\frac{1}{2}\Lambda^2$	$p_0+\frac{1}{2}\Lambda^2$
(i) $Re = 1$				
0	3·87	−2·97	3·87	−2·97
1·0	3·22	−3·34	3·72	−2·84
3·0	−1·07	−7·08	3·43	−2·58
10·0	−47·37	−51·86	2·63	−1·86
(ii) $Re = 40$				
0	0·623	−0·093	0·623	−0·093
0·3	0·563	−0·204	0·608	−0·159
1·0	0·078	−0·665	0·578	−0·165
3·0	−3·951	−4·610	0·549	−0·110

by (27), however for $Re = 1$, $\Lambda = 1$ the computed wake is still quite broad, although it is getting narrower for $\xi_\infty = 4{\cdot}8$. On the other hand the value of ψ_p outside the wake is accurately predicted. For $Re = 40$, $\Lambda = 1$ the wake is quite narrow, but the value outside is overestimated as not enough of the streamlines are closed. The estimate at the higher value of ξ_∞ is better, but there is still scope for improvement. It is worth noting that the major contribution to the minimum value of ψ_p, $(-(2\Lambda + \frac{1}{4}C_D))$, for the case of $Re = 40$, $\Lambda = 1$ comes from the blowing term, as $\frac{1}{4}C_D = 0{\cdot}251$. For $Re = 1$, $\Lambda = 1$ however, $\frac{1}{4}C_D$ is 6·02 and so the drag contribution is larger.

The surface vorticity is plotted in Figure 10 for $Re = 1$ and 40 for various values of Λ. In both cases the rapid fall in surface vorticity with increasing blowing is clear; it is more rapid at $Re = 40$ which is consistent with the fall in C_v shown in Figure 1. Figure 11 shows plots of $p + \frac{1}{2}\Lambda^2$ around the surface of the sphere for the same values of Re and Λ, and the values on the upstream axis ($\theta = \pi$) and downstream axis ($\theta = 0$) are given in Table II. The pressure is supplemented by the blowing correction $\frac{1}{2}\Lambda^2$ so that the comparison of results at different Λ is more transparent; the advantage is apparent from (15). The values for $Re = 1$ are consistent with the steady fall in C_p shown in Figure 1(i); however, the behaviour for $Re = 40$ is more complex, and it is difficult to see that C_p initially increases and then subsequently decreases with increasing Λ.

5. CONCLUSIONS

In this paper we have described accurate finite-element calculations of steady laminar flow past a sphere with a uniform normal blowing velocity over the surface. Particular attention has been paid to the boundary condition applied to the perturbation stream function far from the sphere. The condition (7) that the perturbation stream function should be zero is far less successful than the zero normal derivative condition (8)—with the perturbation stream function set to zero the boundary must be much further from the sphere to achieve a specified accuracy. In addition, the form of the perturbation stream function ψ_p far from the sphere cannot be examined with the condition (7).

From the integral form of the momentum equation, we have shown that the expression for the volume defect in the wake is the sum of the drag contribution found in the absence of blowing and the total mass efflux from the sphere. So the total apparent source far from the sphere and outside the wake is the sum of the drag contribution and twice that due to blowing. The computed values of ψ_p on the outer boundary of the solution region have been compared with the analytic form corresponding to the above result.

We were motivated to carry out these calculations in order to obtain a qualitative measure of the effects of evaporation on the drag on fuel droplets. For the range of Re considered ($1 \leqslant Re \leqslant 100$), blowing always decreasess the drag, and significantly as long as the blowing velocity is comparable to the free stream velocity. This means that an evaporating drop penetrates further into, for example, a furnace than would be predicted by the standard drag law that applies in the absence of blowing.

The pressure and viscous components, C_p and C_v, of the drag coefficient have also been examined. C_v is always drastically reduced by blowing, as the vorticity is blown away from the sphere and the surface value reduced. Indeed for higher values of Re and Λ the maximum vorticity is no longer found on the surface. For low Re, C_p also falls with increasing Λ, although more slowly than C_v, as found in the low Re solution of Dukowicz.[14] For $Re = 40$ and 100 it is found that C_p initially increases, reaches a maximum and then decreases. However, the increase in C_p is much smaller than the fall in C_v, and thus C_D still decreases, contradicting the argument sometimes found in the literature that the fall in C_v is compensated by the rise in C_p, so that the resulting change in C_D is small.

ACKNOWLEDGEMENT

Thanks are due to the U.K. Department of Energy for support of this work, which forms part of the IEA project on Conservation in Combustion.

REFERENCES

1. K. A. Cliffe, D. A. Lever and K. H. Winters, 'A finite difference calculation of spray combustion in turbulent, swirling flow', in R. W. Lewis, and K. Morgan (eds) *Proc. 1st Int. Conf. on Numerical Methods in Thermal Problems*, Swansea, 1979. Pineridge Press, 1979, pp. 447–457.
2. C. T. Crowe, M. P. Sharma and D. E. Stock, 'The particle-source-in cell (PSI-CELL) model for gas-droplet flows', *J. Fluids Eng.*, **99,** 325–332 (1977).
3. A. D. Gosman, E. Ioannides, D. A. Lever and K. A. Cliffe, 'A comparison of "continuum" and "discrete droplet" finite-difference models used in the calculation of spray combustion in swirling, turbulent flows', *Harwell Report TP865/HTFS RS308*, 1980.
4. G. K. Batchelor, *An Introduction to Fluid Dynamics*, Cambridge University Press, 1967.
5. B. Fornberg, 'A numerical study of steady viscous flow past a circular cylinder', *J. Fluid Mech.*, **98,** 819–855 (1980).
6. A. E. Hamielec, T. W. Hoffman and L. L. Ross, 'Numerical studies of the Navier–Stokes equation for flow past spheres I', *A.I.Ch.E.J.*, **13,** 212–219 (1967).
7. B. P. Le Clair, A. E. Hamielec and H. R. Pruppacher, 'A numerical study of the drag on a sphere at low and intermediate Reynolds numbers', *J. Atmos. Sci.*, **27,** 308–315 (1970).
8. S. C. R. Dennis and J. D. A. Walker, 'Calculation of the steady flow past a sphere at low and moderate Reynolds numbers', *J. Fluid Mech.*, **48,** 771–789 (1971).
9. M. Renksizbulut, 'Energetics and dynamics of droplet evaporation in high temperature intermediate Reynolds number flows', *Ph.D. Thesis*, Northwestern University, Evanston, Illinois, 1981.
10. M. Renksizbulut and M. C. Yuen, 'Numerical study of droplet evaporation in a high-temperature stream', *ASME J. Heat Transfer*, **105,** 389–397 (1983).
11. K. A. Cliffe and D. A. Lever, 'Numerical aspects of finite-element calculations of flow past a sphere', in C. Taylor, J. A. Johnson and W. R. Smith (eds) *Proc. 3rd Int. Conf. on Numerical Methods in Laminar and Turbulent Flow*, Seattle, 1983, Pineridge Press, 1983, pp. 25–36.
12. K. A. Cliffe and D. A. Lever, 'A finite-element study of isothermal, laminar flow past a sphere at low and intermediate Reynolds numbers'. *Harwell Report AERE-R 10868*, H.M.S.O., 1983.
13. P. Chuchottaworn, A. Fujinami and K. Asano, 'Numerical analysis of the effect of mass injection or suction on drag coefficients of a sphere', *J. Chem. Eng. Jap.*, **16,** 18–24 (1983).
14. J. K. Dukowicz, 'An exact solution for the drag of a sphere in low Reynolds number flow with strong uniform blowing or suction', *Phys. Fluids*, **25,** 1117–1118 (1982).
15. P. Tong, 'On the solution of the Navier–Stokes equations in two dimensional and axial symmetric problems', *Proc. 1st. Int. Conf. on Finite Element Methods in Flow Problems*, Swansea, 1974, pp. 57–66.
16. K. H. Winters and K. A. Cliffe, 'A finite-element study of driven laminar flow in a square cavity', *Harwell Report AERE-R 9444*, H.M.S.O., 1979.
17. I. Duff, 'MA32—a package for solving sparse unsymmetric systems using the frontal method', *Harwell Report AERE-R 10079*, H.M.S.O., 1981.